Hindawi
International Journal of Energy Research
Volume 2024, Article ID 2459846, 22 pages
https://doi.org/10.1155/2024/2459846

Research Article

Performance Characteristic of Permanent Magnet Linear Generator for Energy Conversion with Renewable Fuels on Free-Piston Engines

Yidi Wei,[1] Zhengxing Zuo,[1] Boru Jia,[1] Zhiyuan Zhang,[1] Huihua Feng,[1] and Kun Liang[2]

[1]*School of Mechanical Engineering, Beijing Institute of Technology, Beijing 100081, China*
[2]*Department of Engineering and Design, University of Sussex, Brighton BN1 9QT, UK*

Correspondence should be addressed to Boru Jia; boru.jia@bit.edu.cn and Huihua Feng; fenghh@bit.edu.cn

Received 20 December 2023; Revised 14 January 2024; Accepted 19 January 2024; Published 31 January 2024

Academic Editor: Rami Reddy Boppella

Renewable fuels attract more attention owing to reduction of both air pollution and greenhouse gas emissions compared to fossil fuels. The free-piston engine generator is a new energy conversion with compact structure, multifuel combustion mode possibility, and less friction loss, and it can be applied to a variety of renewable fuels. This study investigated the effect of operating parameters on power generation and motion characteristics for free-piston engine generator. A test bench and a detailed and validated numerical model of the free-piston engine generator were presented. Results show that with the increase of the average velocity, the output power root mean square (RMS) and efficiency of the generator gradually increase. The output power RMS grows rapidly, whereas the generator efficiency gradually stabilizes. Under the same average velocity but different strokes and frequencies, the generator power and efficiency are the same. This result means that the multiple-point operating condition can achieve the same output power and generator efficiency goals. Moreover, the optimal operating conditions can be selected comprehensively, considering factors such as fuel properties, combustion efficiency, and performance. The influence of the generator on motion characteristics of the system under pure resistive load and high-frequency operation should be noted.

1. Introduction

Internal combustion engines are widely used in automotive, trains, and power plants. Fossil fuels are considered the major energy form in traditional internal combustion engines [1]. However, the CO, CO_2, NO_x, and other product generator by the combustion of fossil fuels bring environmental problems such as the greenhouse effect and global warming [2–4]. The extraction and use of fossil fuels stress natural resources, leading to environmental degradation, including the depletion and disruption of water resources and land use. Therefore, the renewable fuels are widely investigated by researchers, such as hydrogen and ammonia, to replace fossil fuels [5–8].

A free-piston engine generator is a promising power generation system owing to its compact structure, multifuel combustion mode possibility, high power density, and less friction loss [9–11]. Due to the multifuel adaptability of free-piston engine generator, renewable fuels can be promptly employed, converting them into electrical energy [12]. The utilization of free-piston engine generators with renewable fuels holds promising applications across diverse fields, encompassing hybrid vehicles, combined heat and power systems, and power plants. This application has the potential to mitigate carbon emissions associated with the utilization and extraction of fossil fuels, simultaneously reducing dependence on conventional power sources.

In contrast to conventional internal combustion engines with a crank-link mechanism, the distinctive feature of a free-piston engine generator is the linear reciprocating motion. The main components are the combustion cylinder and the linear generator. The linear generator is driven by the gas pressure generated by the combustion in the cylinder to cut the magnetic fled lines to generate electricity. Based on

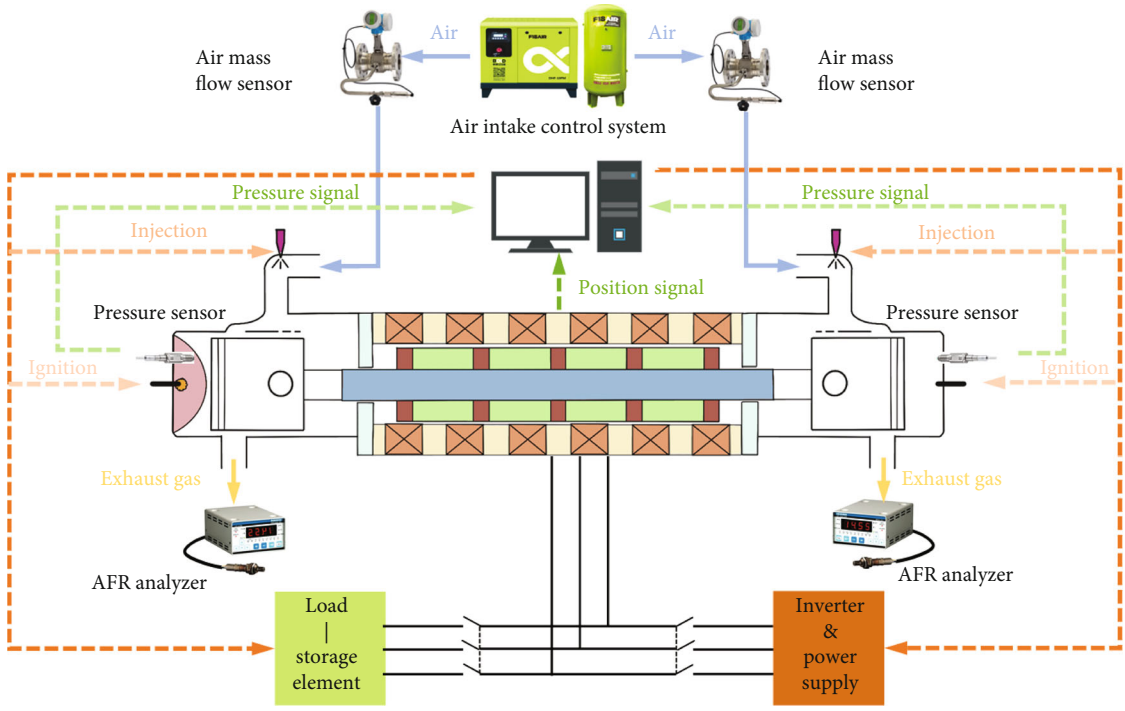

Figure 1: Free-piston engine configuration.

the above two components, a free-piston engine generator has evolved into three dominant structures: single-cylinder, double-cylinder, and opposing types [13].

Introduced the concept of the free-piston engine as early as 1920, which was mainly used as air compressors and gas generators for more than four decades [14]. With the development of power electronical technology and engine control technology, the output form of the free-piston engine has gradually focused on electric energy. The West Virginia University presented a prototype of an ignition two-stroke free-piston generator in 1998 with a cylinder bore of 36.5 mm and a maximum stroke of 50 mm, using a single-phase permanent magnet linear alternator. With an external resistance of 19.5 Ω and an operating frequency of 23.1 Hz, the prototype obtained a maximum output power of 316 W [15–17].

The Sandia National Laboratory has carried out extensive research on compression-ignition free-piston generators since the 1990s [18]. The prototype varies the compression ratio by varying the rate of electrical generation to suit a wide range of fuels. The combustion characteristics of eight fuels, such as propane and natural gas at low equivalence ratios, were explored. The indicated efficiencies can reach 56% because of the nearly constant volume combustion at a high compression ratio [10]. Subsequent research into the effect of the scavenging system on system performance showed that the uniflow scavenging geometry with a low intake pressure can achieve optimum efficiency [19]. An opposing designed prototype with homogeneous charge compression ignition was built in 2013 [20]. Moreover, the alternator is a single-phase moving magnet linear generator designed and fabricated by Magnequench Technology Center of Research Triangle Park, with a stator having 14 coils with a pole pitch of 22 mm and a mover consisting of two 10 mm and four 4 mm permanent magnets [20]. Aichlmayr and Van Blarigan [21] modeled and tested the alternator under pure resistive load, and the simulation and measured voltage and current waveforms had an excellent correspondence.

Roskilly and Mikalsen from the Newcastle University carried out extensive research into the simulation and prototyping of a free-piston engine generator [9, 22]. A coupled dynamic-multidimensional modeling of free-piston engine combustion was proposed. The effect of the top dead center (TDC) position changes the combustion process and engine performance. Moreover, the electric load of generator was proportional to the velocity of the mover in the model, and the output characteristics of the generator were not described [23]. Furthermore, a full-cycle simulation model for the single-piston free-piston engine generator prototype was established to predict the TDC position from the piston velocity in the compression stroke [24]. From the engine control and classical control point of view, the free-piston engine was converted into a SISO system. Compared with the traditional proportional-integral–derivative control method, the pseudoderivative feedback with disturbance feedforward controller (PDF+FF) was adopted, which provided optimum responsiveness and control for the problem of TDC position control because of the step change in the load [25, 26]. The characteristics of ammonia/hydrogen premixed combustion were studied by the chemical kinetics mechanism [27]. The effect of the equivalence ratio, hydrogen blending ratio, and initial pressure on free-piston engine generator characteristics was carried out. The results show that the high-pressure high-temperature environment contributes to reduce NO emission [28].

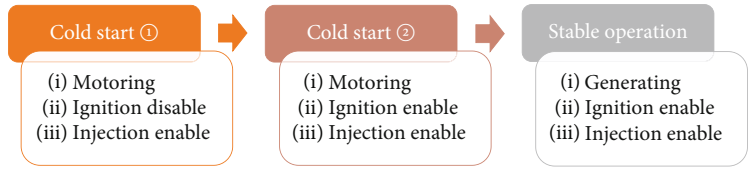

Figure 2: Operating process of free-piston engine.

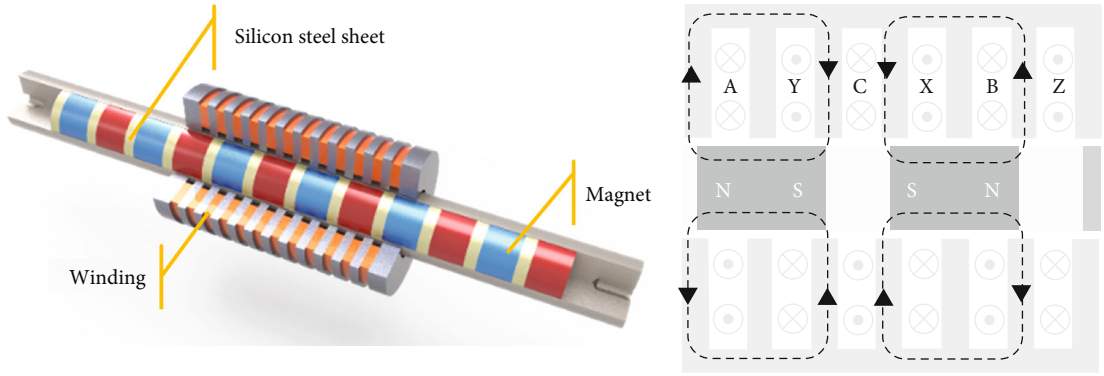

(a) Structure (b) Magnetic circuit

Figure 3: Linear generator configuration.

Toyota Central R&D Labs Inc. proposed a single-cylinder two-stroke combustion system with a linear generator and a gas spring chamber. The three-phase linear generator obtained an output power of 10 kW under the condition of spark ignition combustion (SI) and premixed charged compression ignition combustion (PCCI) in the simulation. In addition, a high thermal efficiency of 42% was achieved in the PCCI combustion case [29]. To ensure the long-term stable operation, a real-time control strategy based on the feedback of piston position and velocity and the control logic with variable feedback gains and customized reference waveform were proposed, which allowed the generator to operate without switching to an electric state [30]. A method to improve the generating efficiency by manipulating the pressure of the air spring chamber was proposed and validated in the prototype [31].

Researchers from the Beijing Institute of Technology have successively developed ignition-type and compression-ignition free-piston prototypes [31–34]. They carried out simulation and experimental research on system cold start control and l cascade control [35–40]. A full-cycle numerical model was proposed to investigate the output characteristics and kinematic properties of a free-piston engine generator, and the efficiency was estimated to be 31.5% at a power output of 4 kW [41].

Research on the power output characteristics of a free-piston engine generator mainly focused on the influence of various structural parameters of the system on the output performance. Ezrann Z. Zainal A investigated the effect of different aspect ratios (1, 1.5, and 2) on the FPLG operating frequency and power output [42] and found that the medium stroke (AR 1.5) had the best overall operating frequency of 5.25 m/s and power root mean square (RMS) 51.4 W. Chen et al. investigated the three-phase, 12-slot/11-pole tubular linear generator equipped with a modular stator winding electromagnetic characteristics through changes in key three-dimensional ratios, such as dimensional ratios $\tau m/\tau p$ and stator and motion ratios with an outer diameter [43]. Aziz et al. explored the effect of five generator stator core configurations (GA, GB, GC, GD, and GD) on the power generation performance, generating an RSM power of 203.9 W with the GB configuration [44]. Lim et al. simulated the back EMF and the cogging forces of a tubular-type linear generator using the finite element method and the Fourier series expansion. They found that the proper pole pitch modulation could reduce the cogging force and increase the back EMF [45]. Abdalla et al. compared the effects of various translator velocities and three different ferromagnetic materials for the stator core, namely, silicon steel laminations, mild steel, and Somaloy on the cogging force of the PMLG. They found that as the translator speed increases, the induced voltage increases [46].

Table 1: Parameters of the permanent magnet tubular linear generator.

Parameters (unit)	Value
Resistance of stator (ph-ph) (Ω)	12.8
Inductance of stator (pH-pH) (mH)	26
Force constant (N/A)	56
Max stator current (A)	20
Max stroke (m)	0.07
Pole pitch (m)	0.02
Back EMF constant (ph-ph) (V/(m/s))	41
Flux linkage of permanent magnets (Wb)	0.27

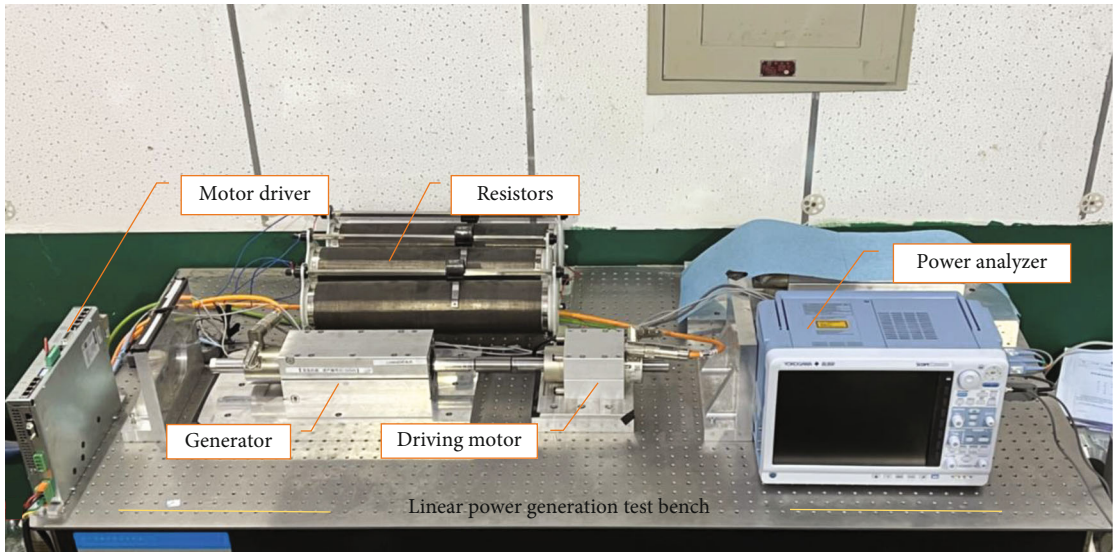

Figure 4: Test bench for the linear generator.

Table 2: List of instruments of the test bench.

Instruments	Type	Technical parameters
Power analyzer	Yokogawa DL5000	0 ~ 150 A; 0 ~ 1.5 kV; ±0.02% FS
Displacement sensor	Linmot P10-70 × 80	0 ~ 70 mm; ±20 μm; ±1 V
Force sensor	HBM U10M	1.25 kN; ±0.02% FS
Data collection	NI PXIe-6356 NI PXIe-8821	1.25 MS/s/channel; 16 bits; 2.6 GHz dual-core
Resistor	PX20-T	0 ~ 50 Ω; 2500 W

Studies on linear generators in a free-piston engine generator mainly focused on the influence of generator and engine structural parameters on generation characteristics. Free-piston engine generators using different renewable fuels need to achieve specific compression ratios and combustion conditions, and the system operating characteristics such as stroke, frequency, and peak velocity presented in the generating stage will also vary within a large range, which affect the system electrical output characteristics. Studies on the influence of free-piston generator operating parameters on generation characteristics and motion characteristics are scarce. A comprehensive analysis of the influence of operational characteristics on the system power output is pivotal in guiding the meticulous selection of components within the rectifier-inverter circuit, ensuring optimal compatibility across various fuel applications. Simultaneously, the identification of key factors influencing system efficiency and power output offers crucial insights for the refinement and optimization of operational conditions. In this study, a free-piston engine generator test bench and detail description model are established to investigate the performance of linear generators under different operating conditions. Through experimental and simulation studies, the impact of operational parameters such as stroke, frequency, and load on the efficiency and power output characteristics of the system has been thoroughly investigated. The findings not only contribute to the advancement of engineering practices, enabling the development of high-performance free-piston engine generators, but also aimed at advancing the application of renewable fuels in these generators, paving the way for a cleaner and more efficient approach to power generation.

2. Linear Generator for Free-Piston Engines

2.1. Free-Piston Engine Configuration. Figure 1 illustrates the construction of a two-stroke free-piston engine. Two cylinders are located on both sides of the body, and a permanent magnet linear generator is located in the middle of the two cylinders. The mover of linear generator, pistons, and connecting rods together form the moving components of the system. The moving component reciprocates within the range of mechanical constraints mainly composed of cylinders and stator.

As shown in Figure 2, the operating process of the system mainly includes the cold start process and the stable operation process. Correspondingly, the linear generator works in the motoring status and generation status. In the early stage of the cold start process, the linear generator works at the motoring status, diving the pistons to reciprocate to compress the gas from the air intake system in the cylinders. Once the ignition condition is met, the system enters the later stage of the cold start process, the ignition

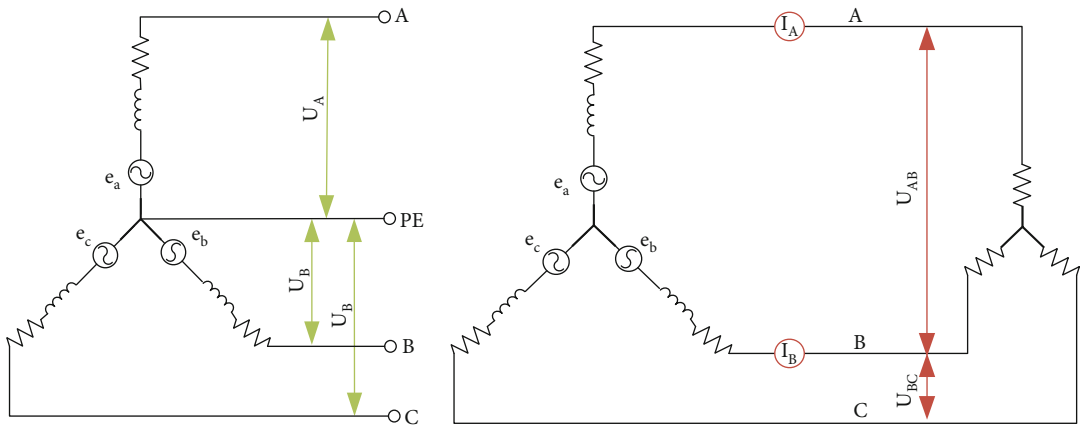

(a) Open circuit (b) Load condition

Figure 5: Test condition.

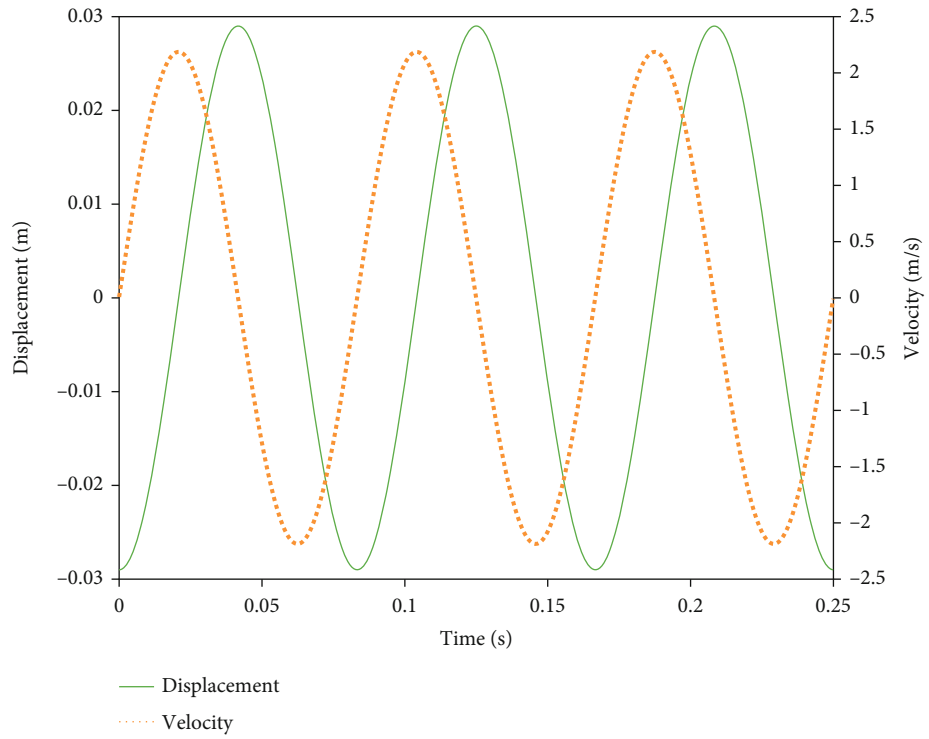

Figure 6: Schematic diagram of velocity and displacement under test conditions.

and fuel injection module are enabled, the linear generator continues to work in the motoring status, and the combustion occurs alternately in the two cylinders. Moreover, the moving component reciprocates under the impetus of gas and generator. As the system movement and combustion gradually stabilize, the linear generator disconnects the inverter, whereas the load or energy storage element is connected. The linear generator also enters the power generation status. The ignition and fuel injection module continuously inject energy into the system. In addition, the alternating combustion process drives the mover's reciprocating motion, cutting the magnetic field lines to produce electrical energy, which is consumed by the load or stored by the energy storage elements. More information about the operating characteristics of the free-piston engine can be found in [41, 47].

2.2. Permanent Magnet Tubular Linear Generator for Application with Free-Piston Engines. A permanent magnet tubular linear generator is used for a free-piston engine, as shown in Figure 3. This generator is mainly composed of a mover composed of magnets and high magnetic permeability silicon steel sheets and a stator composed of three-phase windings. The magnet on the mover adopts the transverse magnetization method, the similar magnetic poles of the adjacent magnets face each other, and a silicon steel sheet

Table 3: List of test operating conditions.

Case number	Load (Ω)	Frequency (Hz)	Stroke (m)
1	—	4	0.01
2	—	4	0.015
3	—	4	0.02
4	—	4	0.025
5	—	4	0.03
6	—	4	0.035
7	—	4	0.04
8	—	4	0.045
9	—	4	0.05
10	—	4	0.055
11	—	4	0.06
12	—	4	0.065
13	—	6	0.01
14	—	6	0.015
15	—	6	0.02
16	—	6	0.025
17	—	6	0.03
18	—	6	0.035
19	—	6	0.04
20	—	6	0.045
21	—	6	0.05
22	—	6	0.055
23	—	6	0.06
24	—	6	0.065
25	—	8	0.01
26	—	8	0.015
27	—	8	0.02
28	—	8	0.025
29	—	8	0.03
30	—	8	0.035
31	—	8	0.04
32	—	8	0.045
33	—	8	0.05
34	—	8	0.055
35	—	8	0.06
36	—	8	0.065
37	—	10	0.01
38	—	10	0.015
39	—	10	0.02
40	—	10	0.025
41	—	10	0.03
42	—	10	0.035
43	—	10	0.04
44	—	10	0.045
45	—	10	0.05
46	—	10	0.055
47	—	10	0.06
48	—	10	0.065

Table 3: Continued.

Case number	Load (Ω)	Frequency (Hz)	Stroke (m)
49	—	12	0.01
50	—	12	0.015
51	—	12	0.02
52	—	12	0.025
53	—	12	0.03
54	—	12	0.035
55	—	12	0.04
56	—	12	0.045
57	—	12	0.05
58	—	12	0.055
59	—	12	0.06
60	—	12	0.065
61	—	14	0.01
62	—	14	0.015
63	—	14	0.02
64	—	14	0.025
65	—	14	0.03
66	—	14	0.035
67	—	14	0.04
68	—	14	0.045
69	—	14	0.05
70	—	14	0.055
71	—	14	0.06
72	—	14	0.065
73	10	4	0.01
74	10	4	0.015
75	10	4	0.02
76	10	4	0.025
77	10	4	0.03
78	10	4	0.035
79	10	4	0.04
80	10	4	0.045
81	10	4	0.05
82	10	4	0.055
83	10	4	0.06
84	10	4	0.065
85	10	6	0.01
86	10	6	0.015
87	10	6	0.02
88	10	6	0.025
89	10	6	0.03
90	10	6	0.035
91	10	6	0.04
92	10	6	0.045
93	10	6	0.05
94	10	6	0.055
95	10	6	0.06
96	10	6	0.065

Table 3: Continued.

Case number	Load (Ω)	Frequency (Hz)	Stroke (m)
97	10	8	0.01
98	10	8	0.015
99	10	8	0.02
100	10	8	0.025
101	10	8	0.03
102	10	8	0.035
103	10	8	0.04
104	10	8	0.045
105	10	8	0.05
106	10	8	0.055
107	10	8	0.06
108	10	8	0.065
109	10	10	0.01
110	10	10	0.015
111	10	10	0.02
112	10	10	0.025
113	10	10	0.03
114	10	10	0.035
115	10	10	0.04
116	10	10	0.045
117	10	10	0.05
118	10	10	0.055
119	10	10	0.06
120	10	10	0.065
121	10	12	0.01
122	10	12	0.015
123	10	12	0.02
124	10	12	0.025
125	10	12	0.03
126	10	12	0.035
127	10	12	0.04
128	10	12	0.045
129	10	12	0.05
130	10	12	0.055
131	10	12	0.06
132	10	12	0.065
133	10	14	0.01
134	10	14	0.015
135	10	14	0.02
136	10	14	0.025
137	10	14	0.03
138	10	14	0.035
139	10	14	0.04
140	10	14	0.045
141	10	14	0.05
142	10	14	0.055
143	10	14	0.06
144	10	14	0.065

Table 3: Continued.

Case number	Load (Ω)	Frequency (Hz)	Stroke (m)
145	15	4	0.01
146	15	4	0.015
147	15	4	0.02
148	15	4	0.025
149	15	4	0.03
150	15	4	0.035
151	15	4	0.04
152	15	4	0.045
153	15	4	0.05
154	15	4	0.055
155	15	4	0.06
156	15	4	0.065
157	15	6	0.01
158	15	6	0.015
159	15	6	0.02
160	15	6	0.025
161	15	6	0.03
162	15	6	0.035
163	15	6	0.04
164	15	6	0.045
165	15	6	0.05
166	15	6	0.055
167	15	6	0.06
168	15	6	0.065
169	15	8	0.01
170	15	8	0.015
171	15	8	0.02
172	15	8	0.025
173	15	8	0.03
174	15	8	0.035
175	15	8	0.04
176	15	8	0.045
177	15	8	0.05
178	15	8	0.055
179	15	8	0.06
180	15	8	0.065
181	15	10	0.01
182	15	10	0.015
183	15	10	0.02
184	15	10	0.025
185	15	10	0.03
186	15	10	0.035
187	15	10	0.04
188	15	10	0.045
189	15	10	0.05
190	15	10	0.055
191	15	10	0.06
192	15	10	0.065

Table 3: Continued.

Case number	Load (Ω)	Frequency (Hz)	Stroke (m)
193	15	12	0.01
194	15	12	0.015
195	15	12	0.02
196	15	12	0.025
197	15	12	0.03
198	15	12	0.035
199	15	12	0.04
200	15	12	0.045
201	15	12	0.05
202	15	12	0.055
203	15	12	0.06
204	15	12	0.065
205	15	14	0.01
206	15	14	0.015
207	15	14	0.02
208	15	14	0.025
209	15	14	0.03
210	15	14	0.035
211	15	14	0.04
212	15	14	0.045
213	15	14	0.05
214	15	14	0.055
215	15	14	0.06
216	15	14	0.065
217	20	4	0.01
218	20	4	0.015
219	20	4	0.02
220	20	4	0.025
221	20	4	0.03
222	20	4	0.035
223	20	4	0.04
224	20	4	0.045
225	20	4	0.05
226	20	4	0.055
227	20	4	0.06
228	20	4	0.065
229	20	6	0.01
230	20	6	0.015
231	20	6	0.02
232	20	6	0.025
233	20	6	0.03
234	20	6	0.035
235	20	6	0.04
236	20	6	0.045
237	20	6	0.05
238	20	6	0.055
239	20	6	0.06
240	20	6	0.065

Table 3: Continued.

Case number	Load (Ω)	Frequency (Hz)	Stroke (m)
241	20	8	0.01
242	20	8	0.015
243	20	8	0.02
244	20	8	0.025
245	20	8	0.03
246	20	8	0.035
247	20	8	0.04
248	20	8	0.045
249	20	8	0.05
250	20	8	0.055
251	20	8	0.06
252	20	8	0.065
253	20	10	0.01
254	20	10	0.015
255	20	10	0.02
256	20	10	0.025
257	20	10	0.03
258	20	10	0.035
259	20	10	0.04
260	20	10	0.045
261	20	10	0.05
262	20	10	0.055
263	20	10	0.06
264	20	10	0.065
265	20	12	0.01
266	20	12	0.015
267	20	12	0.02
268	20	12	0.025
269	20	12	0.03
270	20	12	0.035
271	20	12	0.04
272	20	12	0.045
273	20	12	0.05
274	20	12	0.055
275	20	12	0.06
276	20	12	0.065
277	20	14	0.01
278	20	14	0.015
279	20	14	0.02
280	20	14	0.025
281	20	14	0.03
282	20	14	0.035
283	20	14	0.04
284	20	14	0.045
285	20	14	0.05
286	20	14	0.055
287	20	14	0.06
288	20	14	0.065

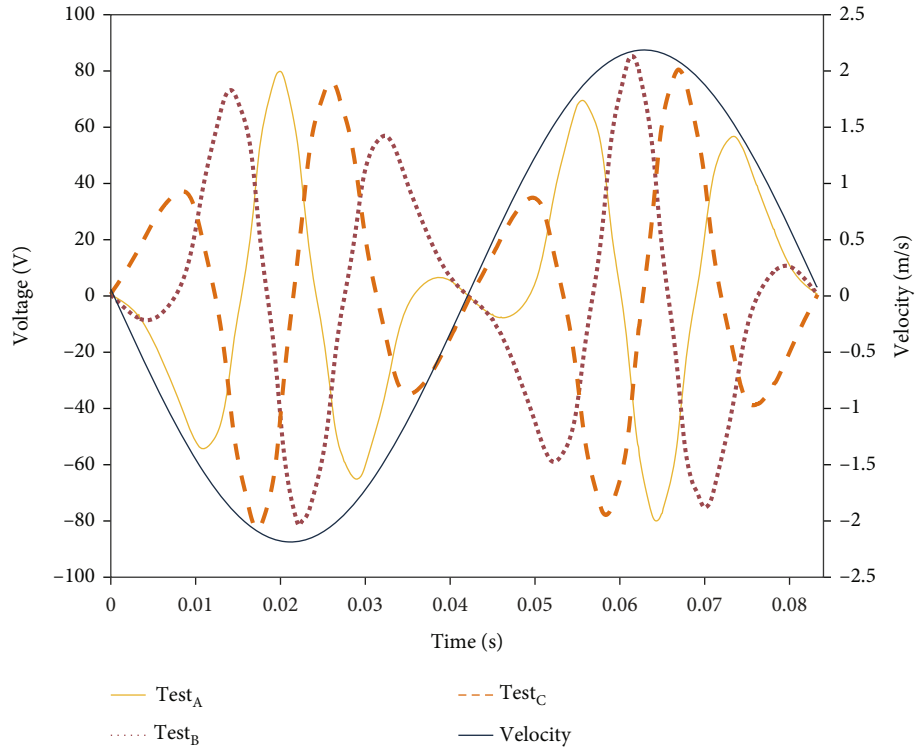

Figure 7: Phase voltage and velocity under open-circuit condition.

exists between the adjacent magnets to conduct magnetism. The stator is mainly made of multiple strands of copper wire wound. The windings are divided into three phases, in which A and C phases are wound in the forward direction, whereas B phases are wound in the opposite direction. Figure 3(b) shows the magnetic circuit. Table 1 presents the key parameters of the permanent magnet tubular linear generator.

A generator model was developed to investigate the kinematic and power generation characteristics of the permanent magnet tubular linear generator in a free-piston engine. The permanent magnet tubular linear generator is modeled in the natural coordinate system based on the following assumptions: (1) ignoring eddy current and hysteresis losses in the generator; (2) ignoring harmonics of the magneto-dynamic potential in the air gap.

The voltage equivalent is shown as follows:

$$V_3 = R_3 I_3 + \frac{\mathrm{d}}{\mathrm{d}t}\Psi_3, \tag{1}$$

where V_3 is the voltage of A, B, and C phases.

$$V_3 = \begin{bmatrix} V_a \\ V_b \\ V_c \end{bmatrix}. \tag{2}$$

R_3 is the resistance of A, B, and C phases.

$$R_3 = \begin{bmatrix} R_a & 0 & 0 \\ 0 & R_b & 0 \\ 0 & 0 & R_c \end{bmatrix}. \tag{3}$$

I_3 is the current of A, B, and C phases.

$$I_3 = \begin{bmatrix} I_a \\ I_b \\ I_c \end{bmatrix}. \tag{4}$$

Ψ_3 is the flux linkage of A, B, and C phases.

$$\Psi_3 = \begin{bmatrix} \Psi_a \\ \Psi_b \\ \Psi_c \end{bmatrix}. \tag{5}$$

The flux linkage of A phase Ψ_a can be expressed as

$$\Psi_a = (L + M) I_a - \varphi_f \sin(\theta + \theta_0), \tag{6}$$

where L is the inductance at the windings, M is the mutual inductance between windings, φ_f is the flux linkage of permanent magnets, θ is the electrical angle corresponding to

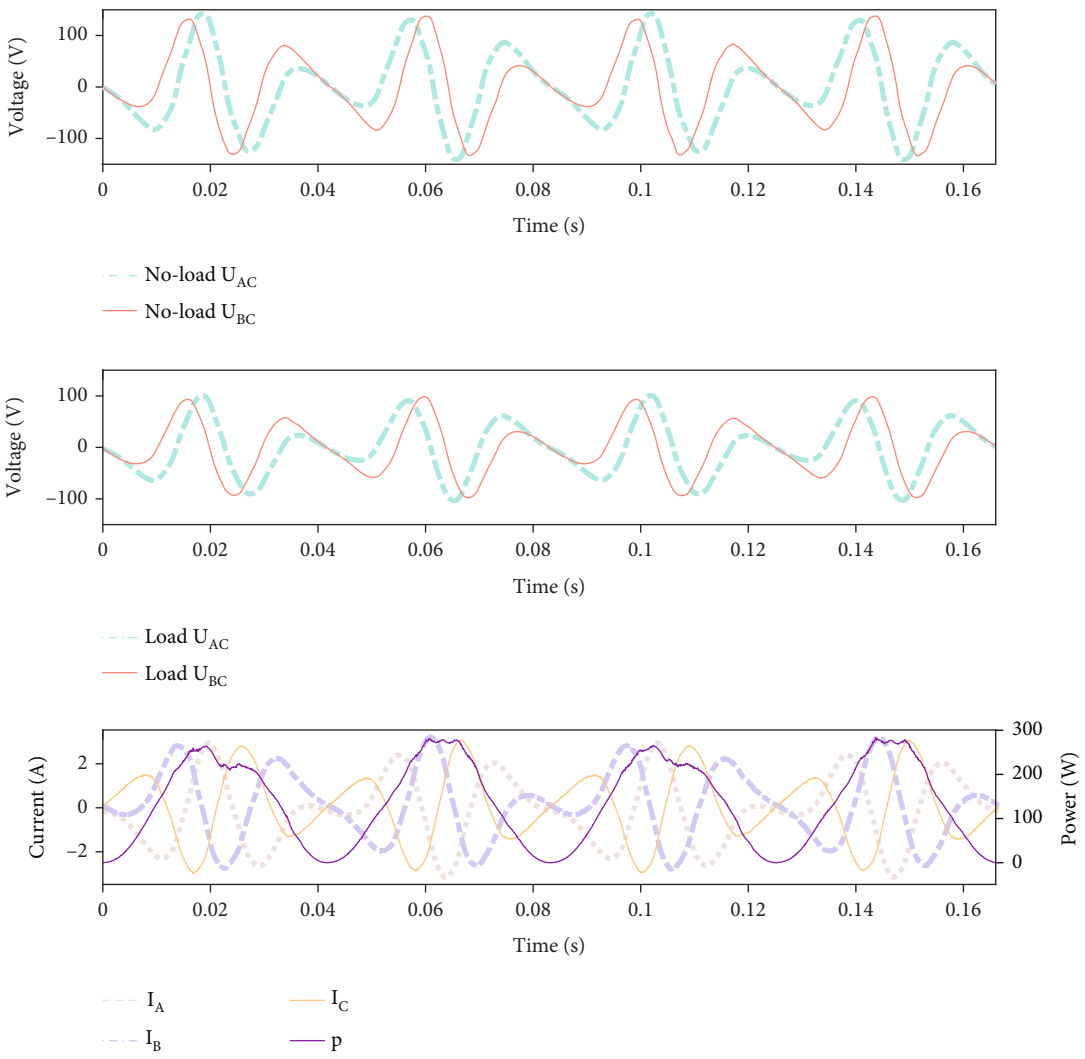

Figure 8: Line voltage and phase current under load conditions.

the position of the mover, and θ_0 represents the initial electrical angle of the mover.

The electrical angle of a linear generator can be calculated by converting the mechanical position. The displacement of the kinematic travel over a pair of poles corresponds to an electrical angle of 360°. The electrical angle for a linear generator can therefore be written as follows:

$$\theta = \frac{\pi}{\tau} x. \tag{7}$$

Therefore, the voltage of the A phase is given by

$$V_a = R_a I_a + (L + M)\dot{I}_a - \varphi_f \frac{\pi \dot{x}}{\tau} \cos\left(\frac{\pi}{\tau} x + \frac{\pi}{\tau} x_0\right). \tag{8}$$

Among them, the back EMF (no-load voltage) of the A phase can be expressed as follows:

$$e_a = -\varphi_f \frac{\pi \dot{x}}{\tau} \cos\left(\frac{\pi}{\tau} x + \frac{\pi}{\tau} x_0\right). \tag{9}$$

The mathematical model in the natural coordinate system is a complex and strongly coupled mutivariable system. For subsequent control and generator analysis, an appropriate coordinate system should be selected to reduce the order and decouple the mathematical model in the natural coordinate system.

To simplify the model, the natural coordinate system (A-B-C axis) should be transformed to the stationary coordinate system (α-β axis) and further to the synchronous motion coordinate system (d-q axis) through the Clark and Park transform.

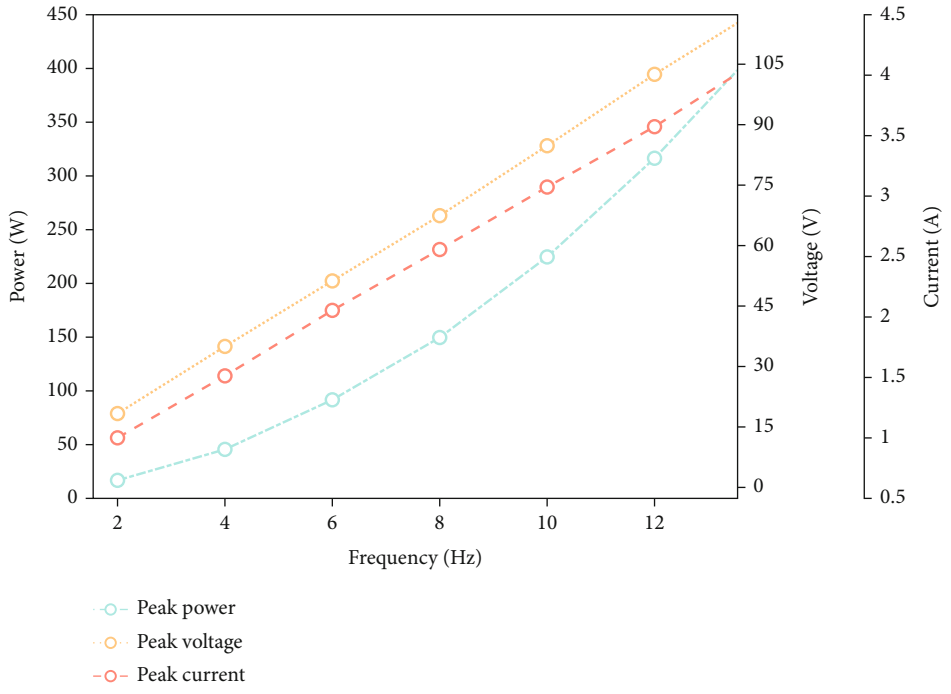

Figure 9: Output characteristics with different frequencies.

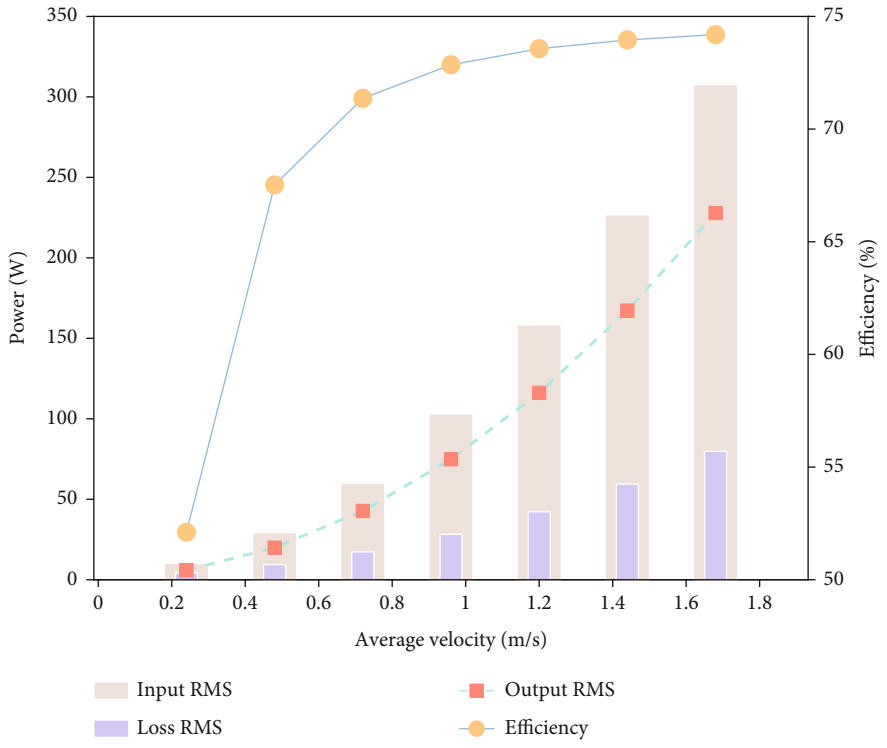

Figure 10: Efficiency and output characteristics with the average velocity.

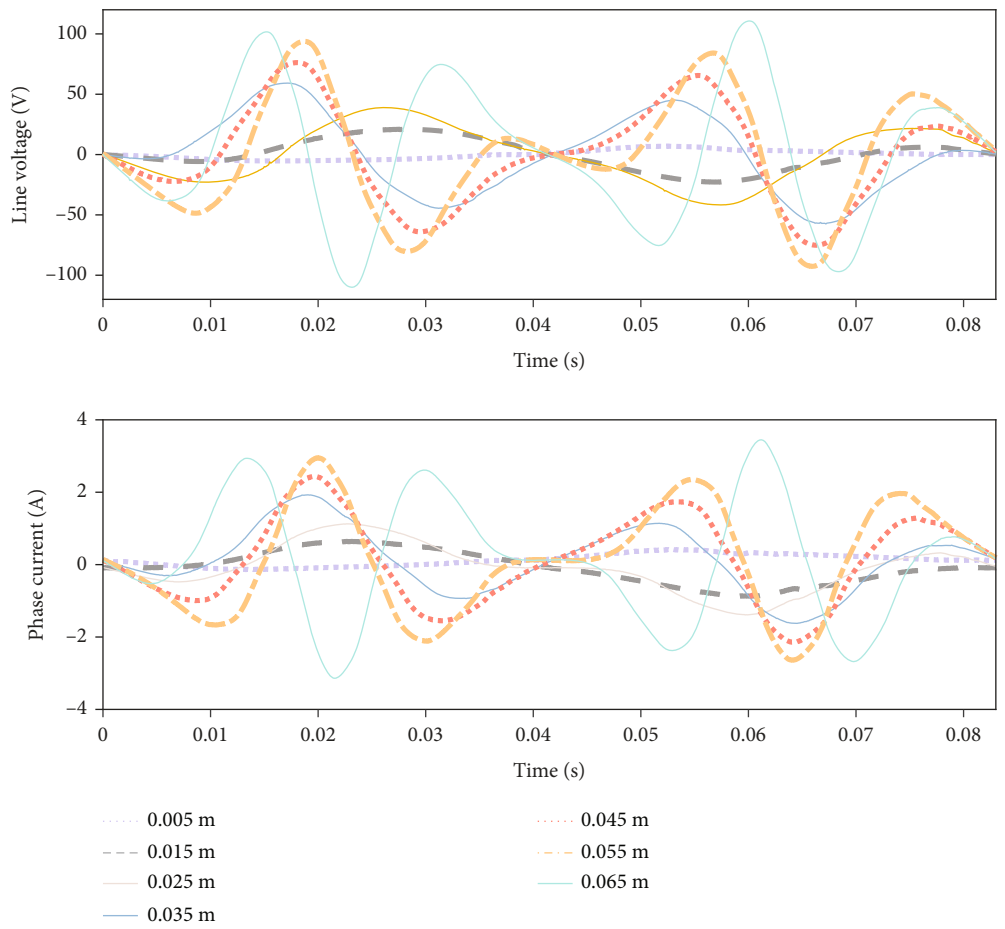

Figure 11: Voltage and current with different strokes.

The conversion of voltage and current from the A-B-C axis to the d-q axis can be expressed as follows:

$$\begin{bmatrix} V_a \\ V_b \\ V_c \end{bmatrix} = \begin{bmatrix} \cos\theta & -\sin\theta & \frac{1}{2} \\ \cos\left(\theta - \frac{2\pi}{3}\right) & -\sin\left(\theta - \frac{2\pi}{3}\right) & \frac{1}{2} \\ \cos\left(\theta + \frac{2\pi}{3}\right) & -\sin\left(\theta + \frac{2\pi}{3}\right) & \frac{1}{2} \end{bmatrix} \begin{bmatrix} V_d \\ V_q \\ 0 \end{bmatrix},$$

$$\begin{bmatrix} I_a \\ I_b \\ I_c \end{bmatrix} = \begin{bmatrix} \cos\theta & -\sin\theta & \frac{1}{2} \\ \cos\left(\theta - \frac{2\pi}{3}\right) & -\sin\left(\theta - \frac{2\pi}{3}\right) & \frac{1}{2} \\ \cos\left(\theta + \frac{2\pi}{3}\right) & -\sin\left(\theta + \frac{2\pi}{3}\right) & \frac{1}{2} \end{bmatrix} \begin{bmatrix} I_d \\ I_q \\ 0 \end{bmatrix}. \tag{10}$$

As the current I_d on the d-axis does not cut the magnetic induction lines when the magnet is in motion, the induced current I_d does not generate the Lorentz force. On the contrary, the$q$-axis is different, which by definition is tangent to the NS center line, and so, it moves to cut the magnetic induction lines. Thus, the induced current I_q generates the Lorentz Force and therefore the thrust force. When calculating thrust in the $d-q$ coordinate system, the thrust will only be related to I_q:

$$F_m = K_i I_q, \tag{11}$$

where K_i is the electromagnetic thrust coefficient of the generator. The above model completes the description of the electrical output characteristics and the force output characteristics of the linear generator.

2.3. Test Bench for Linear Generator. A linear power generation test bench has been established to investigate the generation characteristics of the tubular permanent magnet linear generator on the free-piston engine, as shown in Figure 4. The test bench mainly tested the generator characteristic under open-circuit and resistive load conditions. A permanent magnet tubular linear motor with 36 slots was selected as the drive generator, which reciprocated the linear generator. The mover of the drive motor, the mover of the generator, the force sensor, and the connecting rod formed the moving part of the test bench. The displacement sensor was used for feedback of drive motor control and position acquisition of the moving part. The resistors were used for

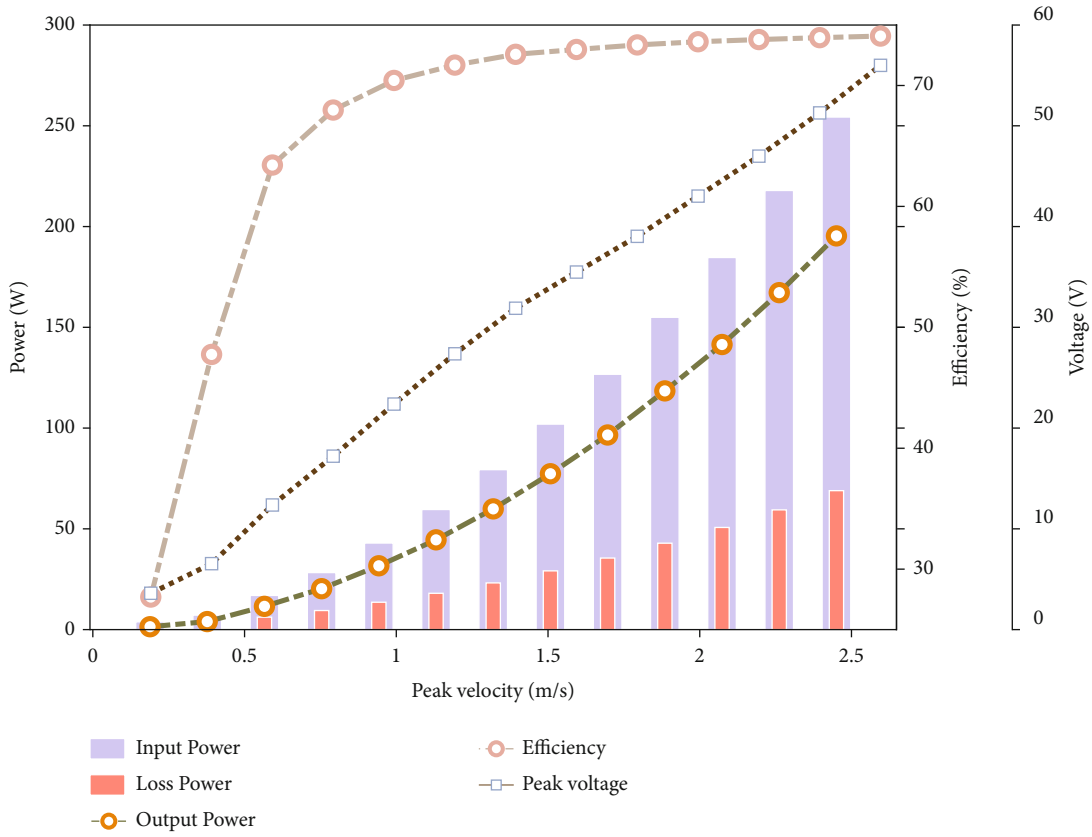

FIGURE 12: Output characteristics with different strokes.

forming a current loop and consuming electrical energy in the resistance load condition. The power analyzer was used to collect the current and the line voltage, calculate the power in the resistance load condition, and collect the no-load voltage at the generator. The force sensor was used to measure the tensile force between the drive motor and the generator. Table 2 presents the list of instruments of the test bench.

In the test bench, the drive motor drives the generator mover to reciprocate sinusoidally with a certain frequency and a certain amplitude to simulate the movement of the generator during the stable operation process of the free-piston generator. As shown in Figure 5(a), when the generator is under no-load condition (open circuit), the three-phase cables of the generator are disconnected, and the phase voltages of the three-phase are collected by a power analyzer. When the generator is in load condition, as shown in Figure 5(b), the resistors are connected in the loop. These resistors were interconnected at one end in a star configuration and grounded, while their other ends were individually connected to the A, B, and C phase outputs of the linear generator. Throughout the resistance variation experiments, the values of the resistors across the three phases were consistently maintained to ensure balance. The power analyzer measures the voltage M_{ac} between A phase and C phase, the voltage M_{bc} between B phase and C phase, and the current I_a of A phase and the current I_b of B phase to calculate the instantaneous power P. The analyzer also calculated the RMS value of power P_{rms} according to the frequency of the mover.

$$P = M_{ac}I_a + M_{bc}I_b,$$
$$P_{\text{rms}} = \sqrt{\frac{1}{T}\int P^2 \mathrm{d}t}. \tag{12}$$

where T is the time to complete one operating cycle.

3. Testing Results

3.1. Testing Conditions. As shown in Figure 6, a sinusoidal motion curve was used to simulate the generator motion under the operating condition free-piston engine. The trajectory is symmetrical with a fixed position as the zero point. In the test, different generation conditions were simulated by changing the motion amplitude and frequency. The stroke of the mover is between 0.01 and 0.065 m, the operating frequency of the mover is between 4 and 14 Hz, and the resistance of resistors is between 10 and 20 Ω, as shown in Table 3. To ensure the accuracy and reproducibility of the experimental results, the aforementioned experimental conditions undergo three repetitions. The subsequent calculations for peak voltage, efficiency, and power are based on the results of 30 consecutive cycles from each experiment, totaling 90 cycles. The experiments are limited by the driving ability of the driving motor, and the maximum stable

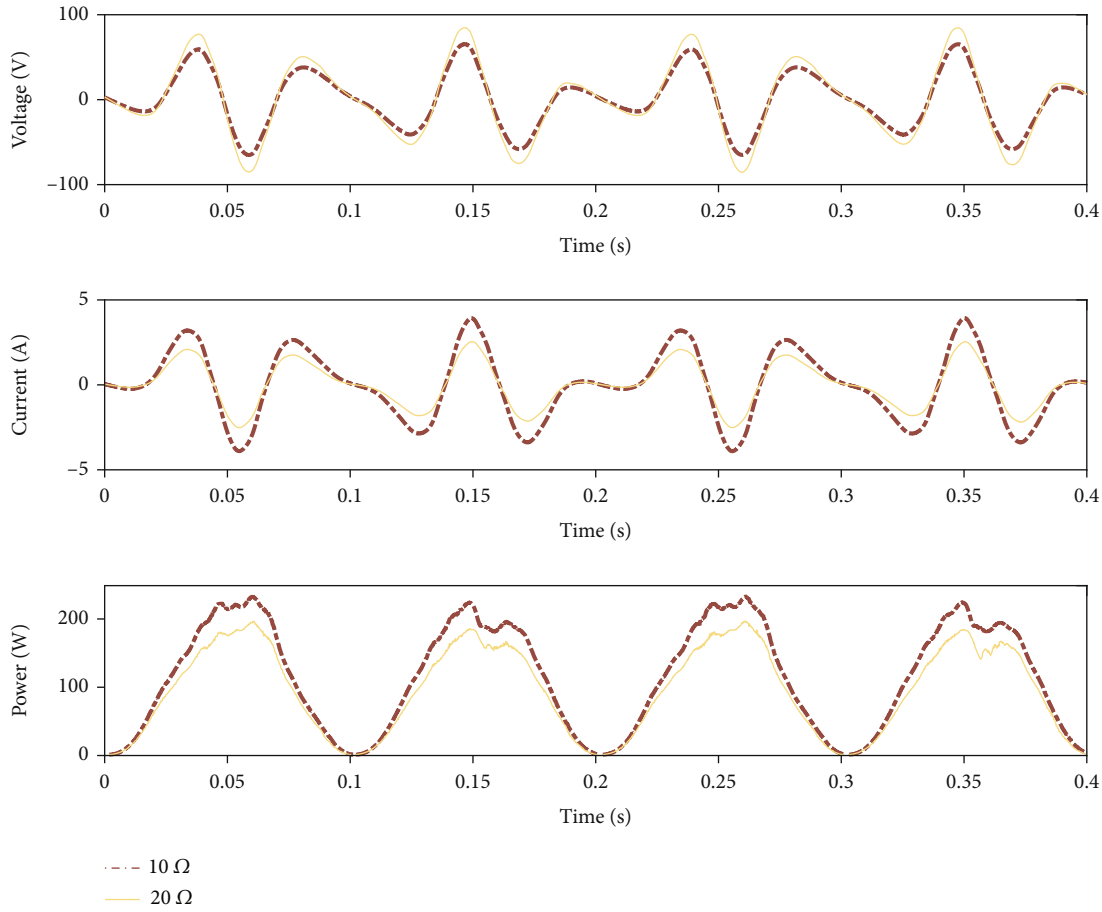

Figure 13: Output characteristics with different resistances.

operating frequency is 14 Hz. In the actual free-piston engine operating conditions, the frequency range is far more than 2–14 Hz. MATLAB/Simulink software was used to simulate and analyze the power generation characteristics of the linear generator to further explore the power generation ability of the linear electric machine at a high operation frequency in Section 4.

3.2. Voltage Output Characteristics with/without Load. Figure 7 shows the three-phase phase voltage and the velocity of the generator working at an operating frequency of 12 Hz and stroke of 0.06 m in the open-circuit test. Multiple periodic variations exist in voltage during a stroke cycle, which are related to the design pole pitch and stroke length of the generator. The voltage of each phase has varying degrees of distortion in different cycles, and the B phase has a maximum peak voltage of 85.3 V in the cycle close to the peak velocity. As the moving velocity of the mover changes continuously within a stroke cycle, the open-circuit phase of each phase has different degrees of distortion in an electrical cycle. The mover always approaches and leaves the dead center at a low velocity, so that the voltage is more distorted in the electrical cycle near the dead center than in the middle of the stroke. At the dead center, the no-load voltage of each phase is zero, and the velocity of the generator is zero. After the movement direction of the mover changes, the phase sequence of the three-phase voltage also changes accordingly. The phase sequence changes from C-B-A to C-A-B. During each velocity reverses, a direction change occurs (sequence reversal), and the frequency and amplitude are modulated, together with the velocity. The peak of the no-load voltage of the linear generator is enveloped by the mover velocity. The conventional no-load voltage description method describes the no-load voltage through the coefficient K_{EMF} and the velocity, which can reflect that the overall change trend of the no-load voltage is proportional to the velocity change trend. However, the detailed description of the voltage, such as voltage distortion rate and electrical cycle, cannot be reflected, which will affect the subsequent power processing process.

Figure 8 illustrates the three-phase phase current, line voltage, and power for a y-connected 20 Ω load. Compared with the line voltage under the no-load condition, the line voltage under the load has a significant drop, and the maximum difference is 47.3 V, which is mainly because of the voltage division of the internal resistance and inductive components. The trend of the three-phase current is the same as the trend of the three-phase voltage under no load, which has multiple periodic changes in the same operation cycle, and the peak current can reach 3.23 A.

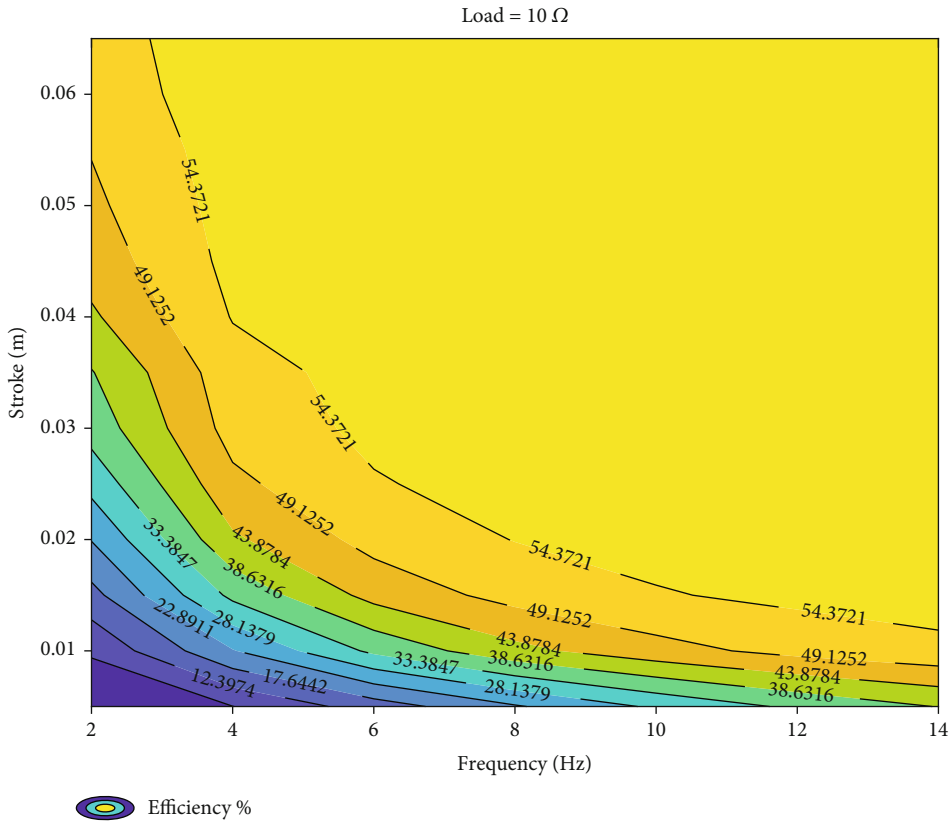

(a) Efficiency map of 10 Ω

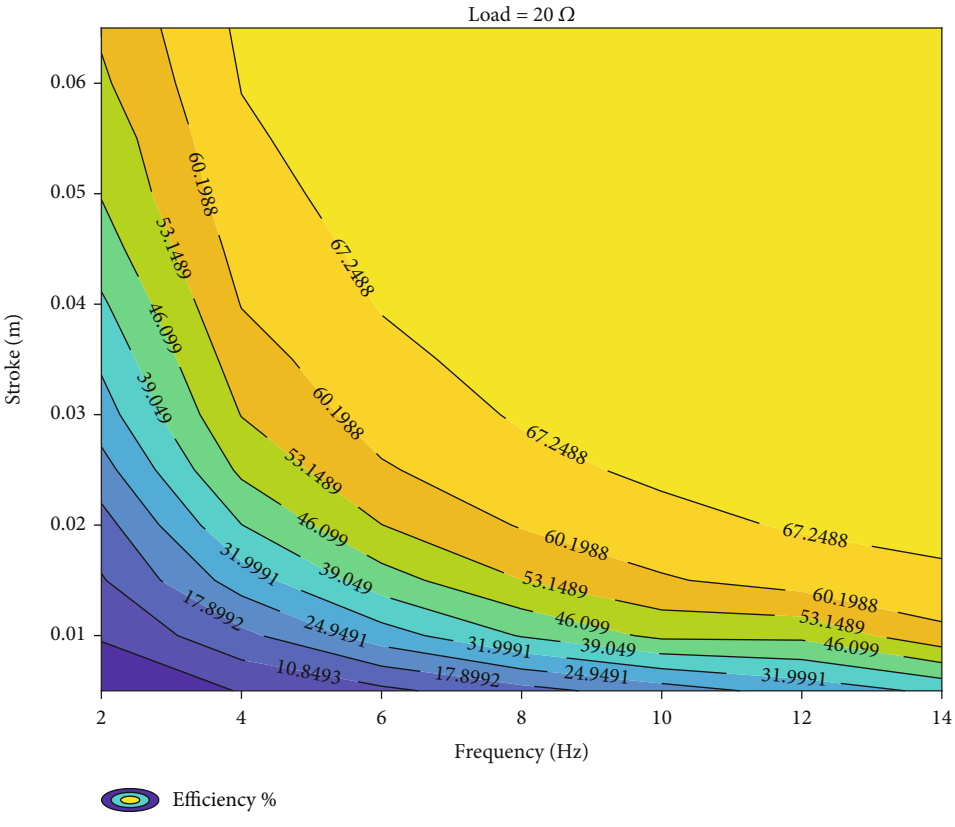

(b) Efficiency map of 20 Ω

Figure 14: Efficiency map with different resistances.

Table 4: Comparison of test and simulation results under different operating conditions.

Frequency (Hz)	Stroke (m)	Peak voltage of experiment (V)	Peak voltage of simulation (V)	Error (V)	Relatively error (%)
14	0.010	17.15	17.24	0.09	0.52
12	0.065	86.99	91.69	4.70	5.40
10	0.070	76.44	82.31	5.87	7.68
8	0.025	21.40	23.31	1.91	8.93
6	0.045	29.45	31.68	2.23	7.57
4	0.035	17.21	17.64	0.43	2.50
2	0.060	13.88	15.17	1.29	9.30

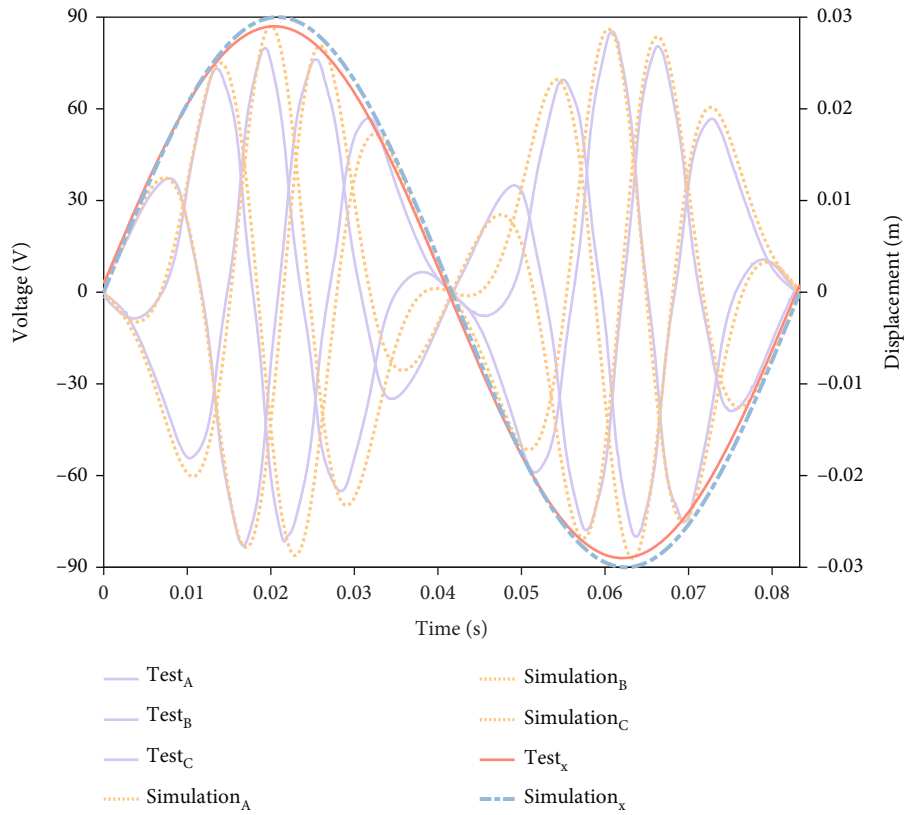

Figure 15: Comparison of phase voltage between test and simulation results.

3.3. Generating Characteristics with Different Frequencies. The free-piston engine can obtain different operating frequencies by varying the operating parameters, such as connecting rod mass and the mixing condition of fuel and gas, giving the generator different characteristics. The output range of the generator will affect the design and match of the rectifier and storage battery. Figure 9 shows the peak value of phase current and line voltage characteristics of the generator at different operating frequencies for a given stroke of 0.06 m. The current and voltage follow the same trend over the operating cycle, with the peak voltage and current increasing with frequency. The peak output power reaches 422.6 W at 14 Hz, with a peak value of phase current of 4.05 A and a peak line voltage of 119.0 V at this operating condition.

The average velocity of the system is an important parameter to evaluate the potential of the engine, which directly affects the dynamic performance, economic performance, mechanical load, thermal load, and vibration and noise of the internal combustion engine. Figure 10 shows the effect of the average velocity on output power loss power and efficiency at different frequencies with the external resistance of 20 Ω. As the input power and loss power are time-varying, the RMS value of the power is used in Figure 10. With the increase of the average velocity, the output power and the loss of the generator are gradually increasing, with a greater increase in output power and a subsequent gradual increase in generator efficiency. At an average velocity of 0.24 m/s, the generator efficiency is only 52.10%, whereas the average velocity reaches 1.68 m/s, the efficiency of the

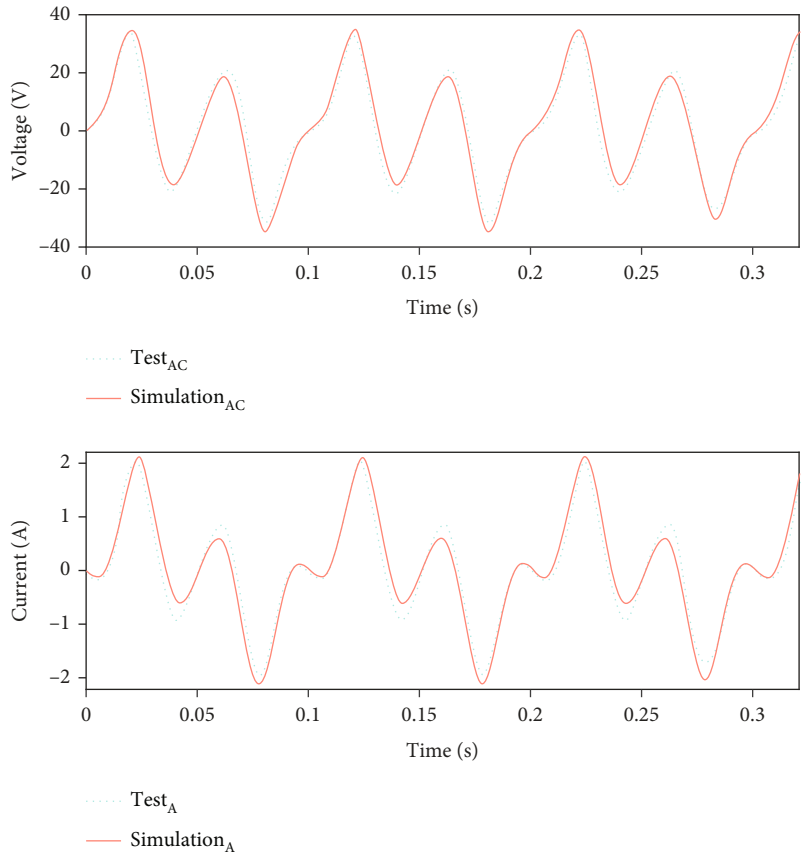

Figure 16: Comparison between test and simulation under load conditions.

generator increases to 74.19%, and the output power RMS is 227.8 W.

3.4. Generating Characteristics with Different Strokes. The free-piston engine is not mechanically limited by crank connecting rods, and the compression ratio can be varied to suit a wide range of fuel and working qualities within the maximum mechanical stroke limit. Therefore, the generator outputs characteristics at different stroke lengths. Figure 11 illustrates the phase current and line voltage variations throughout one operating cycle for different stroke lengths, ranging from 0.005 m to 0.065 m with intervals of 0.01 m, at an operating frequency of 12 Hz. As shown in the phase current waveform, as the stroke increases, the number of times the current crosses the zero point in one operating cycle, that is, the current cycle variation increases in one operating cycle. As the stroke grows, the peak voltage and peak current of the generator also grow gradually because the increase in stroke makes the peak velocity during the operation gradually increase. In addition, as the stroke grows, the distortion rate in the current cycle decreases, and the changes in the current and voltage in the middle of the stroke are closer to sinusoidal.

The increase of the peak velocity of the system will affect the lubrication of the system, which in turn makes friction consumption and others increase. Figure 12 shows the variation of generator efficiency, output power RMS, peak line voltage, and loss power RMS with peak voltage. The peak line voltage is essentially positively correlated with the peak velocity. As in the results of Figure 8, the peak voltage generally appears near the peak velocity. With the increase of the peak velocity, the peak line voltage and output power of the generator gradually increase, but the efficiency gradually tends to be stable at approximately 74%. Further fitting the relationship between peak speed and output power at different frequencies and strokes, the following relationship is obtained:

$$\begin{aligned} U_{\text{peak}} &= 22.98\, V_{\text{peak}}, \\ P_{\text{rms}} &= 32.98\, V_{\text{peak}}{}^{2}, \end{aligned} \tag{13}$$

where V_{peak} is the peak velocity of the mover and U_{peak} is the peak phase voltage of the generator.

The phase current and voltage show different waveforms and trend at different strokes and frequencies. Further analysis of various motion trajectories at the same average velocity (with different strokes and frequencies) shows that the output power RMS efficiencies are similar, which is of great practical importance for a free-piston engine generator to exploit its variable compression ratio characteristics. This notion means that the multiple-point operating condition can achieve the same output power and generator efficiency goals. Moreover, the optimal operating conditions can be

Table 5: Comparison of output characteristics.

Resistance	Test results		Simulation results	
	Output power (RMS)	Efficiency	Output power (RMS)	Efficiency
10 Ω	138.60 W	59.43%	136.97 W	60.98%
15 Ω	126.65 W	69.37%	121.49 W	70.09%
20 Ω	110.29 W	74.30%	106.80 W	75.76%

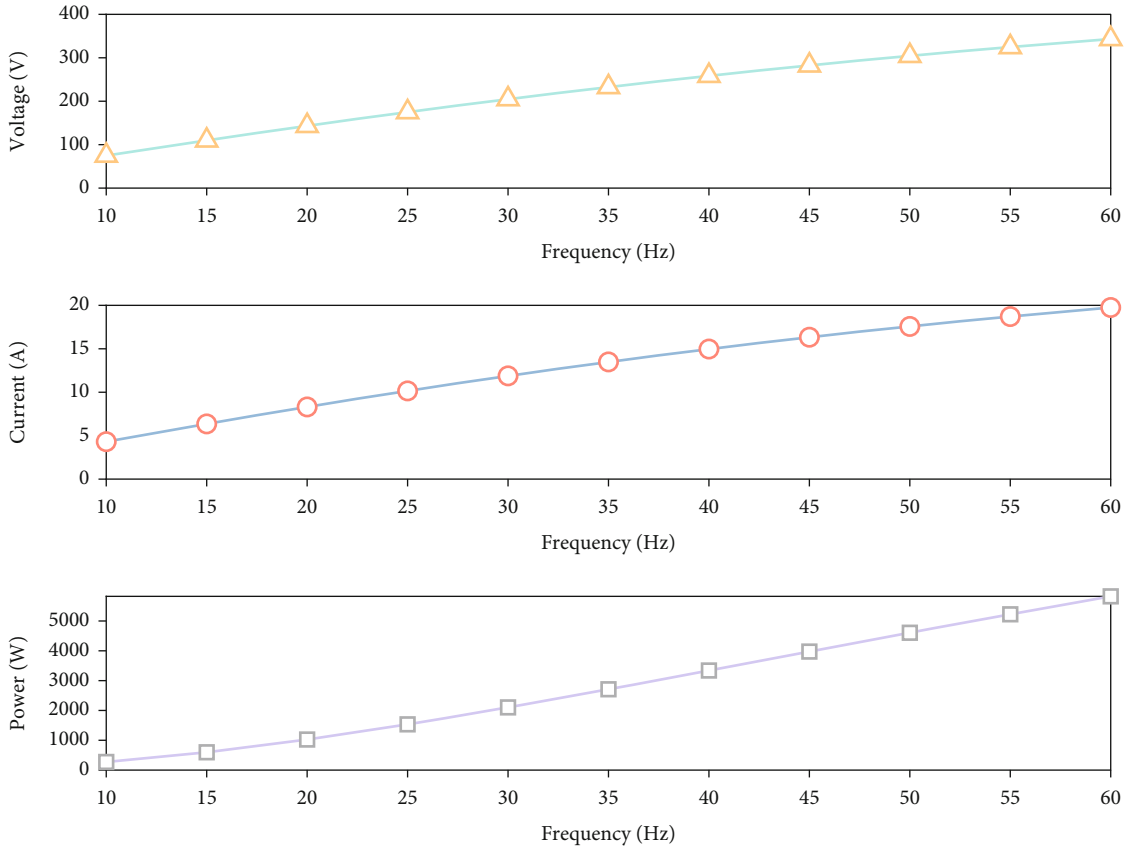

Figure 17: Output characteristics for extended generating characteristics.

selected comprehensively, considering factors such as fuel characteristics, combustion efficiency, and performance.

The test was repeated under the above operating conditions after replacing the external load. Figure 13 shows the variation of the phase current, line voltage, and instantaneous power with the external resistances of 10 and 20 Ω. After reducing the external resistor, the phase voltage has a small drop because of the change in the ratio of the internal and external resistance dividers. On the contrary, the current and instantaneous power increase more significantly where the voltage peaks appear, and the peak instantaneous power appears at the maximum velocity. Compared with the peak power of 196.3 W under 20 Ω, the peak power under 10 Ω is 233.3 W. At the same time, the generator efficiency was calculated, the efficiency under 20 Ω is 73.57%, and the generator efficiency at 10 Ω is 59.43% because its copper loss has been greatly improved. In addition, a high-frequency component can be found near the larger values of the velocity, which is caused by the cogging force.

Figure 14 shows the efficiency map for different resistances, strokes, and frequencies. In the tests carried out, the generator efficiency is the highest at 74.30% under the operating frequency of 14 Hz and the stroke of 0.06 m with the external resistance of 20 Ω. The efficiency for several operating conditions with different strokes and frequencies but the same average velocity and peak velocity was compared. The results show that the efficiency of the generator was the same. The efficiency is directly related to the peak and average velocities. The loss of the generator mainly comes from copper loss. With the increase of the external resistance, the generator efficiency under the same motion conditions can be improved.

4. Simulation Results for Extended Generating Characteristics

The test conditions shown in Table 4 are brought into the simulation model to verify that the simulation model

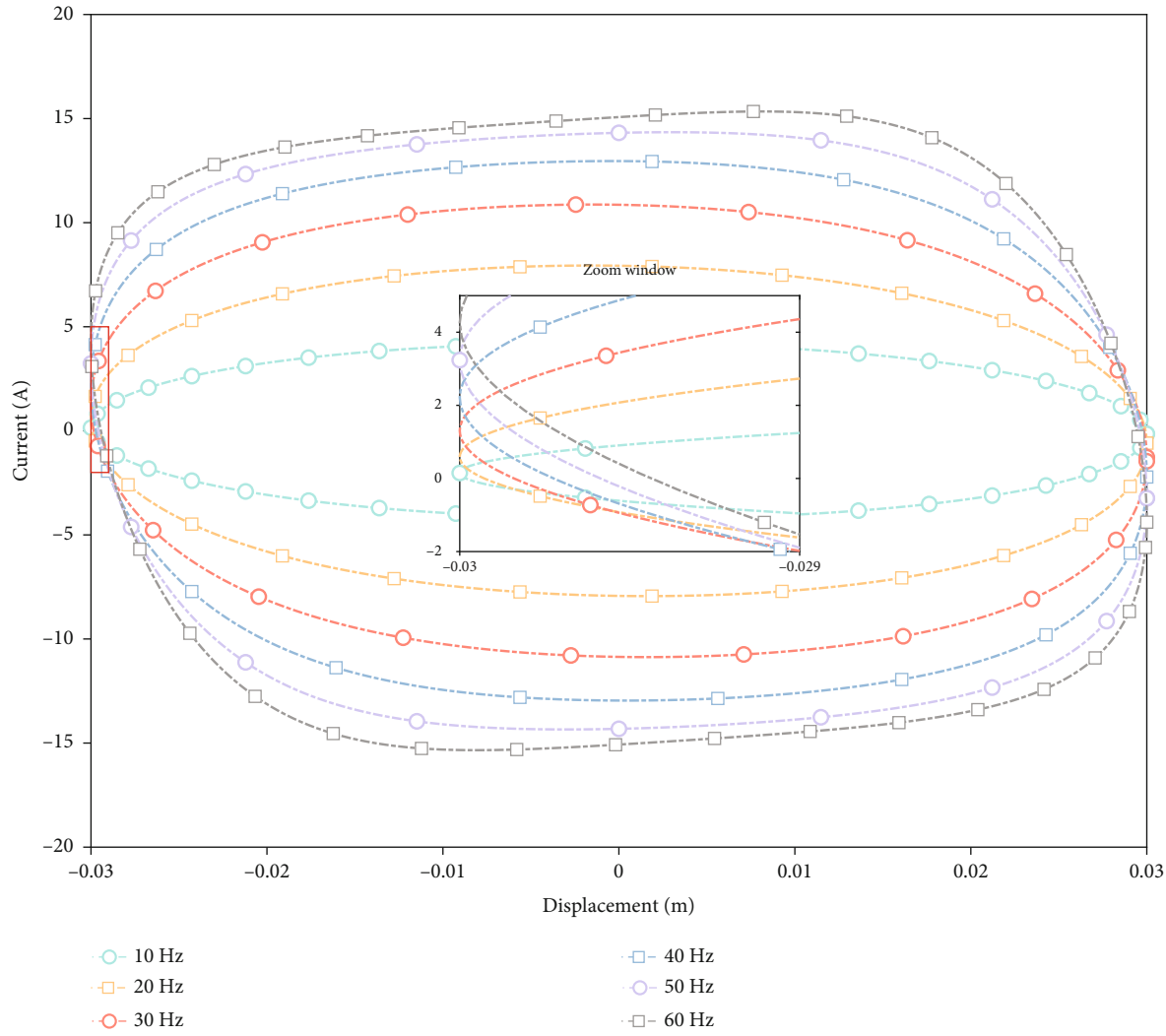

Figure 18: Current of q-axis under different frequencies.

accurately reflects the power generation performance of the linear generator. Figure 15 compares the simulation and experimental results of the open-circuit voltage at the stroke of $S = 0.06$ m when the mover is at the operating frequency of 12 Hz. The modeled results are in good agreement with the experiment, although the error of open-circuit voltage amplitude is 6.1 V. A slight deviation of the initial electrical angle θ_0 between the simulation and the experiment, which play a prominent role in the calculation of the motor flux linkage, and the deviation of the actual stroke from the target stroke caused by the control accuracy of the drive motor may have caused the differences in the voltage peak between the experiment and simulation.

The no-load voltage comparison between simulation and experiment under other working conditions is further compared. Moreover, Table 4 presents the peak voltage value of the A phase in some conditions. The error of the peak voltage between the simulation and experiment under low-frequency short stroke, low-frequency long stroke, and high-frequency short stroke is smaller. By contrast, the error at a long stroke at high frequency and long stroke is large, with a peak voltage error of 5.87 V at a frequency of 10 Hz and a stroke of 0.070 mm. Moreover, Figure 15 shows that in the experimental test, the actual displacement near the top and bottom dead center cannot reach the target position because of the insufficient driving ability and the limited control effect of the driver motor. The tracking error becomes more pronounced as the peak velocity increases in the test.

Figure 16 shows the line voltage and phase current for the generator operating at 10 Hz and 0.03 m with a load resistance of 10 Ω. The simulation results are consistent with the test results. The line voltage and phase current change periodically with the movement of the mover, and the simulation is in great agreement with the experiment. The output power RMS and efficiency under simulation and experiment from the linear generator on the external resistor $R = 10$, 15, and 20 Ω under the operating frequency of 10 Hz with a constant stroke of $S = 0.06$ m were calculated, as shown in Table 5. With the increase of the generator's external resistance, the RMS value of output power decreases continuously, and the error between experiment and simulation is

within 7 W. Simulation and experimental results had the same trend. The maximum deviations of the output power RMS and efficiency were 4.07% and 2.60%, which appear in the 15 and 10 Ω conditions, respectively.

Figure 17 shows that the variation of generator phase voltage, phase current, and peak power at the frequency further increased at 10 Ω with a stroke of 0.06 m. As the frequency increases, the peak voltage and current growth rate of the generator slow down. When the frequency reaches 60 Hz, the peak phase current of the generator reaches 19.19 A, which is close to the maximum instantaneous current allowed by the generator. In this case, the peak phase voltage of the motor is 331.2 V, and the peak power reaches 5.83 kW. The maximum voltage and current limits of the generator depend on the machine thermal properties and the power electronics tolerance to momentary overvoltage and overcurrent conditions. If the current is prolonged overloaded, then the coils or other components will be burnt out.

Figure 18 shows the variation of the q-axis current on the generator side at different frequencies with a displacement over a complete operating cycle. As the frequency increases, the q-axis current of the generator has a similar trend to the phase current, with the current amplitude gradually increasing and the increased range gradually decreasing. The displacement-current curve is elliptical at low frequency, while the displace-velocity curve is also elliptical, and the ratio of q-axis current to velocity can be approximated around a constant. With the increase of the frequency, the displacement-current curve gradually changes, approximating a rhombus. Moreover, the ratio of the q-axis current to velocity can no longer be simply described by a constant. The q-axis current at the dead center at high frequency is no longer near 0 A but gradually deviates from 0 A. The presence of inductance in the circuit makes the inductive reactance larger at high frequency. Therefore, the thrust characteristics of the generator under high-frequency, purely resistive load conditions may change the operating characteristics of the free-piston engine. In addition, the generator force cannot be simply described as proportional to the velocity in the simulation. The power generation characteristics of different load forms and their influence on the system kinematic performance need to be further studied.

5. Conclusions

In this study, the system operating parameters and load parameters of the free-piston engine generator for multiple renewable fuel investigations on the generation and motion characteristics were examined. A linear generator test bench was built to test the generator performance at low frequencies. Moreover, a detailed numerical model of the generator was established and verified through experimental data.

(1) A free-piston engine generator reciprocates during operation. The phase sequence of the generator's phase voltage and phase current will change with the change of the velocity direction. Moreover, the distortion rate of the voltage and current is closely related to the ratio of stroke and tooth pole

(2) Through the test of the generator, as the operating stroke and frequency increase, the power and efficiency of the generation gradually increase, followed by a gradual stabilization of the efficiency. When the operating frequency is 14 Hz, and the stroke is 0.065 m with a load resistance of 20 Ω, the generating power is 489.52 W, and the efficiency is 74.30%.

(3) In the test, the average velocity is directly related to the RMS of generator power. Under the same average velocity but different strokes and frequencies, the generator power and efficiency are the same, which means that multiple-point operating conditions can achieve the same output power and generator efficiency goals. The optimal operating conditions can be selected comprehensively, considering factors such as fuel characteristics, combustion efficiency, and performance

(4) As the frequency increases, owing to the existence of inductive reactance, the q-axis current of the generator is no longer completely positively related to the system velocity. Moreover, the generator force cannot be simply described as proportional to the velocity in the simulation

Nomenclature

e_a: Back electromotive force of A phase (V)
F_m: Motor force (N)
I_3: Matrix of phase current (-)
I_a: Current of A phase (A)
I_b: Current of B phase (A)
I_c: Current of C phase (A)
I_d: Current of d axis (A)
I_q: Current of q axis (A)
I_f: Field current (A)
K_{EMF}: Back EMF coefficient (V/(m/s))
K_i: Electromagnetic thrust coefficient of the generator (N/A)
L: Stator inductance (H)
L_{af}: Mutual inductance at field winding (H)
M: Mutual inductance between stator and mover (H)
M_{ac}: Voltage between A phase and C phase (V)
M_{bc}: Voltage between B phase and C phase (V)
M_f: Field coil (-)
P: Instantaneous power (W)
P_{rms}: RMS value of power (W)
R_3: Matrix of resistance (-)
R_a: Resistance of A phase (Ω)
R_b: Resistance of B phase (Ω)
R_c: Resistance of C phase (Ω)
T: Operating cycle (s)
U_{peak}: Peak phase voltage of the generator (V)
V_3: Matrix of phase voltage (-)
V_a: Voltage of A phase (V)
V_b: Voltage of B phase (V)
V_c: Voltage of C phase (V)
V_d: Voltage of d axis (V)
V_{peak}: Peak velocity of the mover (m/s)

V_q: Voltage of q axis (V)
x: Mover displacement (m)
x_0: Initial mover displacement (m)
$\dot{x}$: Mover velocity (m/s)
θ_0: Initial electrical angle (rad)
θ: Electrical angle (rad)
τ: Pole pitch (m)
Ψ_3: Matrix of flux linkage (-)
Ψ_a: Flux linkage of A phase (Wb)
Ψ_b: Flux linkage of B phase (Wb)
Ψ_c: Flux linkage of C phase (Wb).

Data Availability

Data will be made available on request.

Conflicts of Interest

The authors declare that there is no conflict of interest regarding the publication of this paper.

References

[1] Y. Zhu, Y. Wang, X. Zhen et al., "The control of an opposed hydraulic free piston engine," *Applied Energy*, vol. 126, pp. 213–220, 2014.

[2] M. P. Hekkert, F. H. Hendriks, A. P. Faaij, and M. L. Neelis, "Natural gas as an alternative to crude oil in automotive fuel chains well-to-wheel analysis and transition strategy development," *Energy Policy*, vol. 33, no. 5, pp. 579–594, 2005.

[3] A. Kowalewicz and M. Wojtyniak, "Part D: Journal of automobile engineering," *Alternative Fuels and their Application to Combustion Engines*, vol. 219, no. 1, pp. 103–125, 2005.

[4] A. Cernat, C. Pana, N. Negurescu, G. Lazaroiu, C. Nutu, and D. J. S. Fuiorescu, "Hydrogen—an alternative fuel for automotive diesel engines used in transportation," *Sustainability*, vol. 12, no. 22, p. 9321, 2020.

[5] A. T. Raheem, A. R. A. Aziz, S. A. Zulkifli, M. B. Baharom, A. T. Rahem, and W. B. Ayandotun, "Optimisation of operating parameters on the performance characteristics of a free piston engine linear generator fuelled by CNG-H_2 blends using the response surface methodology (RSM)," *International Journal of Hydrogen Energy*, vol. 47, no. 3, pp. 1996–2016, 2022.

[6] W. B. Ayandotun, A. R. A. Aziz, Z. A. B. Abdul Karim, S. E. Mohammed, and M. A. Ismael, "Investigation on the combustion and performance characteristics of a DI free piston linear generator engine fuelled with CNG-CO2 blend," *Applied Thermal Engineering*, vol. 198, 2021.

[7] Y. Woo, Y. Lee, and Y. Lee, "The performance characteristics of a hydrogen-fuelled free piston internal combustion engine and linear generator system," *International Journal of Low-Carbon Technologies*, vol. 4, no. 1, pp. 36–41, 2009.

[8] F. Huang and W. Kong, "Effect of hydrogen addition on the operating characteristics of a free piston linear engine," *International Journal of Hydrogen Energy*, vol. 45, no. 30, pp. 15402–15413, 2020.

[9] N. B. Hung, "A review of free-piston linear engines," *Applied Energy*, vol. 178, pp. 78–97, 2016.

[10] B. Jia, R. Mikalsen, A. Smallbone, and A. P. Roskilly, "A study and comparison of frictional losses in free-piston engine and crankshaft engines," *Applied Thermal Engineering*, vol. 140, pp. 217–224, 2018.

[11] C. Guo, Z. Zuo, H. Feng, B. Jia, and T. J. A. E. Roskilly, "Review of recent advances of free-piston internal combustion engine linear generator," *Applied Energy*, vol. 269, article 115084, 2020.

[12] R. Mikalsen and A. P. Roskilly, "A review of free-piston engine history and applications," *Applied Thermal Engineering*, vol. 27, no. 14-15, pp. 2339–2352, 2007.

[13] P. A. Achten, *A review of free piston engine concepts*, SAE transactions, 1994.

[14] S. Nandkumar, *Two-Stroke Linear Engine*, West Virginia University, 1998.

[15] D. Rerkpreedapong, *Field Analysis and Design of a Moving Iron Linear Alternator for Use with Linear Engine*, West Virginia University, 1999.

[16] S. Petreanu, *Conceptual Analysis of a Four-Stroke Linear Engine*, West Virginia University, 2001.

[17] S. S. Goldsborough and P. Van Blarigan, *A numerical study of a free piston IC engine operating on homogeneous charge compression ignition combustion*, SAE transactions, 1999.

[18] P. Van Blarigan, N. Paradiso, and S. J. S. T. P. Goldsborough, *Homogeneous charge compression ignition with a free piston: a new approach to ideal Otto cycle performance, No. 982484*, SAE Technical Paper, 1998.

[19] S. S. Goldsborough and P. Van Blarigan, *Optimizing the scavenging system for a two-stroke cycle, free piston engine for high efficiency and low emissions: a computational approach*, SAE transactions, 2003.

[20] M. T. Leick and R. W. Moses, *Experimental evaluation of the free piston engine-linear alternator (FPLA)*, Sandia National Lab. (SNL-NM), Albuquerque, NM (United States), 2015.

[21] H. T. Aichlmayr and P. Van Blarigan, "Modeling and experimental characterization of a permanent magnet linear alternator for free-piston engine applications," *Energy Sustainability*, vol. 48890, pp. 761–770, 2009.

[22] R. Mikalsen and A. P. Roskilly, "The design and simulation of a two-stroke free-piston compression ignition engine for electrical power generation," *Applied Thermal Engineering*, vol. 28, no. 5-6, pp. 589–600, 2008.

[23] R. Mikalsen and A. P. Roskilly, "Coupled dynamic–multidimensional modelling of free-piston engine combustion," *Applied Energy*, vol. 86, no. 1, pp. 89–95, 2009.

[24] R. Mikalsen, E. Jones, and A. P. Roskilly, "Predictive piston motion control in a free-piston internal combustion engine," *Applied Energy*, vol. 87, no. 5, pp. 1722–1728, 2010.

[25] R. Mikalsen and A. P. Roskilly, "The control of a free-piston engine generator. Part 1: Fundamental analyses," *Applied Energy*, vol. 87, no. 4, pp. 1273–1280, 2010.

[26] R. Mikalsen and A. J. A. E. Roskilly, "The control of a free-piston engine generator. Part 2: Engine dynamics and piston motion control," *Applied Energy*, vol. 87, no. 4, pp. 1281–1287, 2010.

[27] F. Zhang, G. Chen, D. Wu, T. Li, Z. Zhang, and N. Wang, "Characterising premixed ammonia and hydrogen combustion for a novel Linear Joule Engine Generator," *International Journal of Hydrogen Energy*, vol. 46, no. 44, pp. 23075–23090, 2021.

[28] F. Zhang, G. Chen, D. Wu, T. Li, Z. Zhang, and N. Wang, "Characteristics of ammonia/hydrogen premixed combustion

in a novel Linear Engine Generator," *In Proceedings*, vol. 58, no. 1, p. 2, 2020.

[29] H. Kosaka, T. Akita, K. Moriya et al., *Development of free piston engine linear generator system part 1-investigation of fundamental characteristics*, SAE Technical Paper, 2014.

[30] S. Goto, K. Moriya, H. Kosaka et al., *Development of free piston engine linear generator system part 2-investigation of control system for generator*, SAE Technical Paper, 2014.

[31] K. Moriya, S. Goto, T. Akita, H. Kosaka, Y. Hotta, and K. Nakakita, *Development of free piston engine linear generator system part3-novel control method of linear generator for to improve efficiency and stability*, SAE Technical Paper, 2016.

[32] J. Mao, Z. Zuo, and H. Feng, "Parameters coupling designation of diesel free-piston linear alternator," *Applied Energy*, vol. 88, no. 12, pp. 4577–4589, 2011.

[33] J. Mao, Z. Zuo, and W. Li, "Multi-dimensional scavenging analysis of a free-piston linear alternator based on numerical simulation," *Applied Energy*, vol. 88, no. 4, pp. 1140–1152, 2011.

[34] H. Feng, Z. Zhang, B. Jia, Z. Zuo, A. Smallbone, and A. P. Roskilly, "Investigation of the optimum operating condition of a dual piston type free piston engine generator during engine cold start-up process," *Applied Thermal Engineering*, vol. 182, article 116124, 2021.

[35] B. Jia, Z. Zuo, H. Feng, G. Tian, A. Smallbone, and A. P. Roskilly, "Effect of closed-loop controlled resonance based mechanism to start free piston engine generator: Simulation and test results," *Applied Energy*, vol. 164, pp. 532–539, 2016.

[36] B. Jia, Z. Zuo, H. Feng, G. Tian, and A. P. Roskilly, "Investigation of the starting process of free-piston engine generator by mechanical resonance," *Energy Procedia*, vol. 61, pp. 572–577, 2014.

[37] B. Jia, G. Tian, H. Feng, Z. Zuo, and A. P. Roskilly, "An experimental investigation into the starting process of free-piston engine generator," *Applied Energy*, vol. 157, pp. 798–804, 2015.

[38] H. Feng, C. Guo, B. Jia, Z. Zuo, Y. Guo, and T. Roskilly, "Research on the intermediate process of a free-piston linear generator from cold start-up to stable operation: Numerical model and experimental results," *Energy Conversion and Management*, vol. 122, pp. 153–164, 2016.

[39] B. Jia, R. Mikalsen, A. Smallbone, Z. Zuo, H. Feng, and A. P. Roskilly, "Piston motion control of a free-piston engine generator: A new approach using cascade control," *Applied energy*, vol. 179, pp. 1166–1175, 2016.

[40] B. Jia, A. Smallbone, H. Feng, G. Tian, Z. Zuo, and A. P. Roskilly, "A fast response free-piston engine generator numerical model for control applications," *Applied energy*, vol. 162, pp. 321–329, 2016.

[41] B. Jia, Z. Zuo, G. Tian, H. Feng, and A. P. Roskilly, "Development and validation of a free-piston engine generator numerical model," *Energy Conversion and Management*, vol. 91, pp. 333–341, 2015.

[42] E. Z. Zainal A, M. A. Ismael, A. R. A. Aziz et al., "Effect of aspect ratio on frequency and power generation of a free-piston linear generator," *Applied Thermal Engineering*, vol. 192, article 116944, 2021.

[43] J. Chen, Y. Liao, C. Zhang, and Z. Jiang, "Design and Ananysis of a Permanent Magnet Linear Generator for a Free-Piston Energy Converter," in *2014 9th IEEE Conference on Industrial Electronics and Applications*, Hangzhou, China, 2014.

[44] A. Aziz, A. Rashid, M. A. Ismael, S. E. Mohammed, M. B. Baharom, and A. R. T. Anwarudin, "Effect of generator configuration on the free-piston motion and power generation of air-driven expander system," *Alexandria Engineering Journal*, vol. 61, no. 4, pp. 3093–3104, 2022.

[45] J. Lim, S.-K. Hong, and H.-K. Jung, "Design and analysis of 5 kw class tubular type linear generator for free-piston engine," *International Journal of Applied Electromagnetics and Mechanics*, vol. 35, no. 4, pp. 231–240, 2011.

[46] I. Abdalla, A. E. Zainal, N. Ramlan, A. Aziz, and M. Heikal, "Cogging force investigation of a free piston permanent magnet linear generator," in *IOP Conference Series: Materials Science and Engineering*, vol. 257, article 012055, IOP Publishing, 2017.

[47] Y. Wei, Z. Zuo, B. Jia et al., "Operating characteristics of a linear range extender with different energy consumption topologies," *Applied Thermal Engineering*, vol. 230, article 120743, 2023.